days after PHx. Subsequently, nonparenchymal cells were isolated, immunostained, and analyzed. This analysis revealed that LSEC proliferation was dramatically reduced in the absence of Ang2 (Fig. 4A). Hepatocyte-derived vascular endothelial growth factor (VEGF) is known to act as a potent stimulus for LSEC proliferation (*25*). However, serum VEGF levels were similar in WT and Ang2-deficient mice 2 and 4 days after PHx (fig. S13). Candidate-based gene expression screening revealed that VEGF receptor 2 (VEGFR2) expression in LSEC was decreased by 60% in Ang2-deficient mice (Fig. 4B). Expression of the transcription factor Id1, which acts downstream of VEGFR2, was unchanged in the absence of Ang2 (fig. S14). However, the expression of Wnt2, a hepatotropic angiocrine factor whose expression is controlled by VEGFR2 signaling (*3*), was markedly reduced in Ang2-deficient LSECs during the angiogenic phase (fig. S14).

We further validated that Ang2 regulated VEGFR2 expression in cultured human endothelial cells (HUVECs). Ang2 silencing significantly reduced mRNA and protein levels of VEGFR2 (Fig. 4C and fig. S15A). Moreover, Ang2 overexpression led to increased VEGFR2 expression (fig. S15B). Conversely, silencing of the Ang2 receptor Tie2 increased VEGFR2 expression, indicating that Ang2-regulated VEGFR2 expression was Tie2-dependent (Fig. 4D). In line with the Ang2-regulated VEGFR2 expression, Ang2 silencing not only reduced HUVEC proliferation but also inhibited HUVEC migration and delayed wound closure (Fig. 4, E and F, and figs. S16 and S17). Consistently, migration of cultured LSEC from Ang2-deficient mice was similarly impaired (fig. S18).

This study was aimed at elucidating angiocrine mechanisms of liver regeneration. After the identification of Ang2 as a key vascular-derived regulator of liver regeneration, we hypothesized that similar paracrine cross-talk mechanisms may be operative during chronic liver injury. To study this hypothesis, WT and Ang2-deficient mice were treated with CCl_4. Chronic liver injury was evident by a rough liver surface, collagen deposits, and elevated serum levels of aspartate aminotransferase (AST) and alanine aminotransferase (ALT) (fig. S19, A, B, and E). Sirius red and cleaved Caspase-3 staining showed similar levels of collagen deposits and hepatocyte apoptosis in both genotypes (fig. S19, B to D). Serum levels of AST, ALT, and alkaline phosphatase (AP) also showed no significant differences (fig. S19E). Nonetheless, hepatocytes of Ang2-deficient mice showed ~2.5 times higher proliferation rates as compared with that of hepatocytes of WT mice (fig. S19, F and G).

LSEC-derived Ang2 is required to spatiotemporally orchestrate the proliferation of hepatocytes and LSEC to efficiently restore liver structure and function after hepatectomy (Fig. 4G): The rapid down-regulation of Ang2 after hepatectomy regulates hepatocyte proliferation in a paracrine (angiocrine) manner by down-regulating LSEC TGFβ1 production, removing an endogenous growth inhibitory mechanism. During the angiogenic phase, recovery of Ang2 expression controls LSEC proliferation by regulating VEGFR2 expression in an autocrine manner. The dynamics of these divergent indirect and direct two-compartment effects are strictly controlled by the temporal regulation of LSEC Ang2 expression during liver regeneration (rapid down-regulation after hepactectomy and gradual recovery during the later angiogenic phase). Previous studies have shown that LSECs support liver regeneration in a stimulatory manner by secreting hepatotropic cytokines, including HGF and Wnt2 (*3*, *9*). In this study, we establish that LSECs control liver regeneration in a much more dynamic manner through stimulatory and inhibitory effects. These data indicate a general mechanism by which signals transmitted from LSECs to hepatocyte play critical and rate-limiting roles in orchestrating liver regeneration. Collectively, the data shed fundamental insights into the role of the endothelium as a gatekeeper and regulator of tissue homeostasis and regeneration.

References and Notes

1. E. Lammert, O. Cleaver, D. Melton, *Science* **294**, 564–567 (2001).
2. K. Matsumoto, H. Yoshitomi, J. Rossant, K. S. Zaret, *Science* **294**, 559–563 (2001).
3. B. S. Ding *et al.*, *Nature* **468**, 310–315 (2010).
4. B. S. Ding *et al.*, *Cell* **147**, 539–553 (2011).
5. R. Taub, *Nat. Rev. Mol. Cell Biol.* **5**, 836–847 (2004).
6. S. Hoehme *et al.*, *Proc. Natl. Acad. Sci. U.S.A.* **107**, 10371–10376 (2010).
7. G. K. Michalopoulos, *Am. J. Pathol.* **176**, 2–13 (2010).
8. G. K. Michalopoulos, *J. Cell. Physiol.* **213**, 286–300 (2007).
9. J. LeCouter *et al.*, *Science* **299**, 890–893 (2003).
10. C. Daly *et al.*, *Cancer Res.* **73**, 108–118 (2013).
11. H. G. Augustin, G. Y. Koh, G. Thurston, K. Alitalo, *Nat. Rev. Mol. Cell Biol.* **10**, 165–177 (2009).
12. U. Fiedler *et al.*, *Blood* **103**, 4150–4156 (2004).
13. H. Oh *et al.*, *J. Biol. Chem.* **274**, 15732–15739 (1999).
14. U. Fiedler *et al.*, *Nat. Med.* **12**, 235–239 (2006).
15. G. K. Michalopoulos, M. C. DeFrances, *Science* **276**, 60–66 (1997).
16. Y. Miyaoka *et al.*, *Curr. Biol.* **22**, 1166–1175 (2012).
17. N. W. Gale *et al.*, *Dev. Cell* **3**, 411–423 (2002).
18. J. J. Maher, *J. Clin. Invest.* **91**, 2244–2252 (1993).
19. E. M. Webber, J. Bruix, R. H. Pierce, N. Fausto, *Hepatology* **28**, 1226–1234 (1998).
20. R. Sun, B. Jaruga, S. Kulkarni, H. Sun, B. Gao, *Biochem. Biophys. Res. Commun.* **338**, 1943–1949 (2005).
21. S. B. Jakowlew *et al.*, *Cell Regul.* **2**, 535–548 (1991).
22. Y. Shi, J. Massagué, *Cell* **113**, 685–700 (2003).
23. M. Pibiri *et al.*, *FASEB J.* **15**, 1006–1013 (2001).
24. R. S. Chari, D. T. Price, S. R. Sue, W. C. Meyers, R. L. Jirtle, *Am. J. Surg.* **169**, 126–132 (1995).
25. E. Taniguchi, S. Sakisaka, K. Matsuo, K. Tanikawa, M. Sata, *J. Histochem. Cytochem.* **49**, 121–129 (2001).

Acknowledgments: We thank G. Thurston (Regeneron, Tarrytown, NY) for providing Ang2-deficient mice and critical discussions. We also thank A. Budnik and S. Savant (DKFZ Heidelberg, Germany) for important discussions and comments on the manuscript. We gratefully acknowledge the excellent technical support of F. Bestvater and M. Brom of the Microscopy Facility, M. Bewerunge-Hudler of the Microarray Unit, and the DKFZ laboratory animal core facility. This work was supported by grants from the Deutsche Forschungsgemeinschaft (SFB-TR23 "Vascular Differentiation," SFB-TR77 "HCC," and SFB873 "Stem Cell Biology"), the DKFZ-MOST Cancer Research Cooperation, and the EU FP7 "SYSTEMAGE" (all to H.G.A.). H.G.A. is supported by an endowed chair from the Aventis Foundation. Microarray data were deposited in the Gene Expression Omnibus (GEO) database (accession no. GSE50046).

Supplementary Materials

www.sciencemag.org/content/343/6169/416/suppl/DC1
Materials and Methods
Figs. S1 to S20
Tables S1 to S3
References (*26*–*29*)
Movies S1 and S2

19 August 2013; accepted 12 December 2013
10.1126/science.1244880

Single β-Actin mRNA Detection in Neurons Reveals a Mechanism for Regulating Its Translatability

Adina R. Buxbaum,[1,2] Bin Wu,[1,2] Robert H. Singer[1,2,3,4]*

The physical manifestation of learning and memory formation in the brain can be expressed by strengthening or weakening of synaptic connections through morphological changes. Local actin remodeling underlies some forms of plasticity and may be facilitated by local β-actin synthesis, but dynamic information is lacking. In this work, we use single-molecule in situ hybridization to demonstrate that dendritic β-actin messenger RNA (mRNA) and ribosomes are in a masked, neuron-specific form. Chemically induced long-term potentiation prompts transient mRNA unmasking, which depends on factors active during synaptic activity. Ribosomes and single β-actin mRNA motility increase after stimulation, indicative of release from complexes. Hence, the single-molecule assays we developed allow for the quantification of activity-induced unmasking and availability for active translation. Further, our work demonstrates that β-actin mRNA and ribosomes are in a masked state that is alleviated by stimulation.

More than a century ago, Ramón y Cajal postulated that memories could be stored by modifying the shape and, consequently, the strength of synaptic connections between neurons (*1*). In our current understanding of learning and memory formation, synaptic plasticity

expressed as activity-induced changes in synapse morphology and, subsequently, in signaling strength constitutes one of the physical manifestations of memory formation (*2*). In postsynaptic forms of plasticity, activity-induced morphological remodeling and enhanced synaptic transmission can be specific to a single dendritic spine (*3*) and can require both protein synthesis (*4*) and increased polymerization of the cytoskeletal protein β-actin (*5*). Local protein synthesis provides a mechanism of achieving spatial specificity of synaptic modification that can persist over time (*6*). β-actin mRNA localization in neuronal dendrites is essential for proper dendritic spine structure and abundance (*7*, *8*), suggesting that regulation of β-actin protein concentration through local translation plays a role in synaptic plasticity.

Because β-actin mRNA is abundant in neurons (*9*), mRNAs must be maintained in a repressed state in the vicinity of synapses with translation factors readily available as needed for local translation. Physical sequestration of localized mRNAs in large neuronal RNA granule structures may serve to repress the mRNAs. RNA granules have been described as large, dense, neuronal-specific structures composed of ribosomes; mRNAs, including β-actin mRNA; and translation factors (*10*, *11*). Putatively, local activity induces granule disassembly, spatially restricting translation to stimulated synapses (*10*, *12*). To date, there exists little evidence that granules regulate mRNA functionality. With the use of single-molecule imaging of endogenous β-actin mRNA and ribosomes, we provide evidence that the availability of β-actin mRNA to translation factors is transiently regulated by synaptic activity.

Single mRNA fluorescent in situ hybridization (FISH) analysis provided an absolute quantitation of dendritic mRNAs in cultured hippocampal neurons (*13*) (fig. S1). Probe hybridization efficiency to single molecules was calibrated with the brightness of a single probe (*14*). By this method, we found that dendritic mRNAs bind only half of the expected probes (Fig. 1, A and D, and fig. S2). However, exposure to chemical long-term potentiation (cLTP) induction, known to result in enlarged spines (*15*), increased probe binding to the expected number (11) and doubled detection of β-actin mRNAs along dendrites within 10 to 15 min (Fig. 1, B, D, and E; fig. S2, A and

[1]Department of Anatomy and Structural Biology, Albert Einstein College of Medicine, 1300 Morris Park Avenue, Bronx, NY 10461, USA. [2]Gruss Lipper Biophotonics Center, Albert Einstein College of Medicine, 1300 Morris Park Avenue, Bronx, NY 10461, USA. [3]Dominick P. Purpura Department of Neuroscience, Albert Einstein College of Medicine, 1300 Morris Park Avenue, Bronx, NY 10461, USA. [4]Janelia Farm Research Campus, Howard Hughes Medical Institute, Ashburn, VA 20147, USA.

*Corresponding author. E-mail: robert.singer@einstein.yu.edu

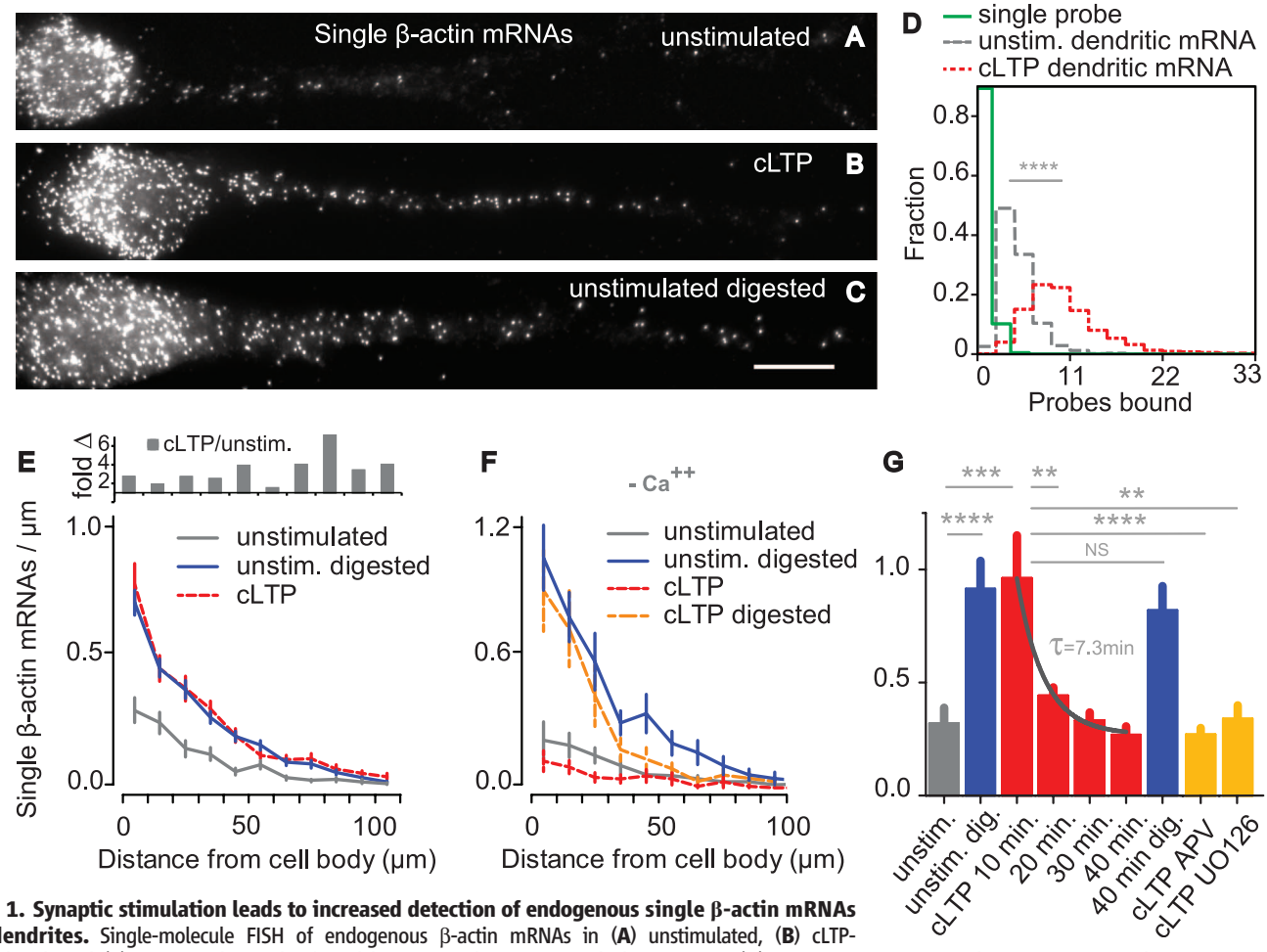

Fig. 1. Synaptic stimulation leads to increased detection of endogenous single β-actin mRNAs in dendrites. Single-molecule FISH of endogenous β-actin mRNAs in (**A**) unstimulated, (**B**) cLTP-stimulated, and (**C**) protease-digested cultured hippocampal neurons. Scale bar, 10 μm. (**D**) Histogram of integrated intensities of single β-actin mRNAs in dendrites. After cLTP, single mRNAs bind the expected number of probes, although half without stimulation (unstim.) [****$P < 0.0001$ (cLTP $n = 2728$ mRNAs, 25 cells; unstim. $n = 665$ mRNAs, 19 cells; single FISH probes $n = 2131$)]. (**E**) Single β-actin mRNAs per micrometer in dendrites. Fold increase of mRNA density along unstimulated to stimulated dendrites (top). From top to bottom in key: $n = 26$, 97, or 57 dendrites. (**F**) Single β-actin mRNAs per micrometer in dendrites with removal of extracellular calcium (from top to bottom: $n = 23$, 12, 19, or 7 dendrites). (**G**) Mean single mRNAs per micrometer in the first 50 μm of dendrites. cLTP-induced unmasking of mRNA decays with a time constant (τ) of 7.3 min (fit: coefficient of determination $R^2 = 0.996$). Digestion 40 min after cLTP shows no decrease in mRNA, consistent with mRNA repackaging ($P = 0.5$). Increased mRNA detection is blocked by NMDA receptor inhibition (APV) or MEK1/2 inhibition (UO126) (**$P < 0.01$, ***$P = 0.001$, ****$P < 0.0001$; Student's t test). In order from left to right: $n = 26$, 21, 21, 35, 47, 44, 32, 31, or 23 dendrites. NS, not significant; dig., digested. Error bars in (E) to (G) denote SEM.

C; and fig. S3). Inefficient mRNA detection suggested inaccessibility of probes to dendritic mRNA, whereas stimulation induces unmasking. In contrast to neurons, β-actin mRNAs in glial cells in the same field hybridized the expected number of probes, irrespective of stimulation (fig. S2B). Probes to the β-actin 3′ untranslated region (3′ UTR), as well as the open reading frame, demonstrated mRNA unmasking (fig. S2, C and D). Increased mRNA was not due to transport from the soma or transcription (fig. S2, E to G).

If mRNA was masked by a proteinaceous complex, a limited prehybridization proteolytic digestion step would be expected to enhance mRNA detection. A protease digestion protocol was devised (*16*) that increased detectable β-actin mRNAs in dendrites equivalent to levels after stimulation (Fig. 1E). Poly(A) mRNA detection in dendrites also increased upon digestion (fig. S2H), suggesting that additional mRNAs may be masked in neurons.

To be physiologically regulated, mRNA unmasking would require signaling cascades that occur during synaptic activity. Inhibition of *N*-methyl-D-aspartate (NMDA) receptor activity with 2-amino-5-phosphonopentanoic acid (APV), inhibition of MEK1/2 (mitogen-activated protein kinase kinase 1 and 2) with UO-126, or depletion of calcium from the extracellular medium prevented increased mRNA detection during cLTP (Fig. 1, F and G), relating mRNA unmasking to local metabolic changes that occur during synaptic plasticity. Detectable dendritic β-actin mRNA peaked at 10 min after cLTP and returned to baseline within 30 min (Fig. 1G), indicating that the default condition is masking. Furthermore, limited mRNA availability for translation after cLTP could provide for a burst of protein synthesis.

Because repressive RNA granule complexes in neurons are composed of densely packed ribosomes (*11*), ribosomes may also be unmasked during cLTP. Similar to mRNA, cLTP increased endogenous ribosomal RNA (rRNA) detection along dendrites, as did sample digestion (Fig. 2A and fig. S4, A to E). Ribosomal particle intensities in protease-treated neuronal dendrites were nonhomogeneous and contained denser regions when compared with glia (fig. S4, F to H). Consistent with dispersal of ribosomes during unmasking, cLTP decreased the abundance of bright dendritic rRNA structures (fig. S4, E and I, and fig. S5F). To determine whether β-actin mRNA and ribosomes may be associated in the same particle as previously reported (*11*, *17*), we performed dual-color hybridization in protease digested neurons (Fig. 2B). More than 30% of β-actin mRNAs colocalized with neuron-specific bright ribosomal structures.

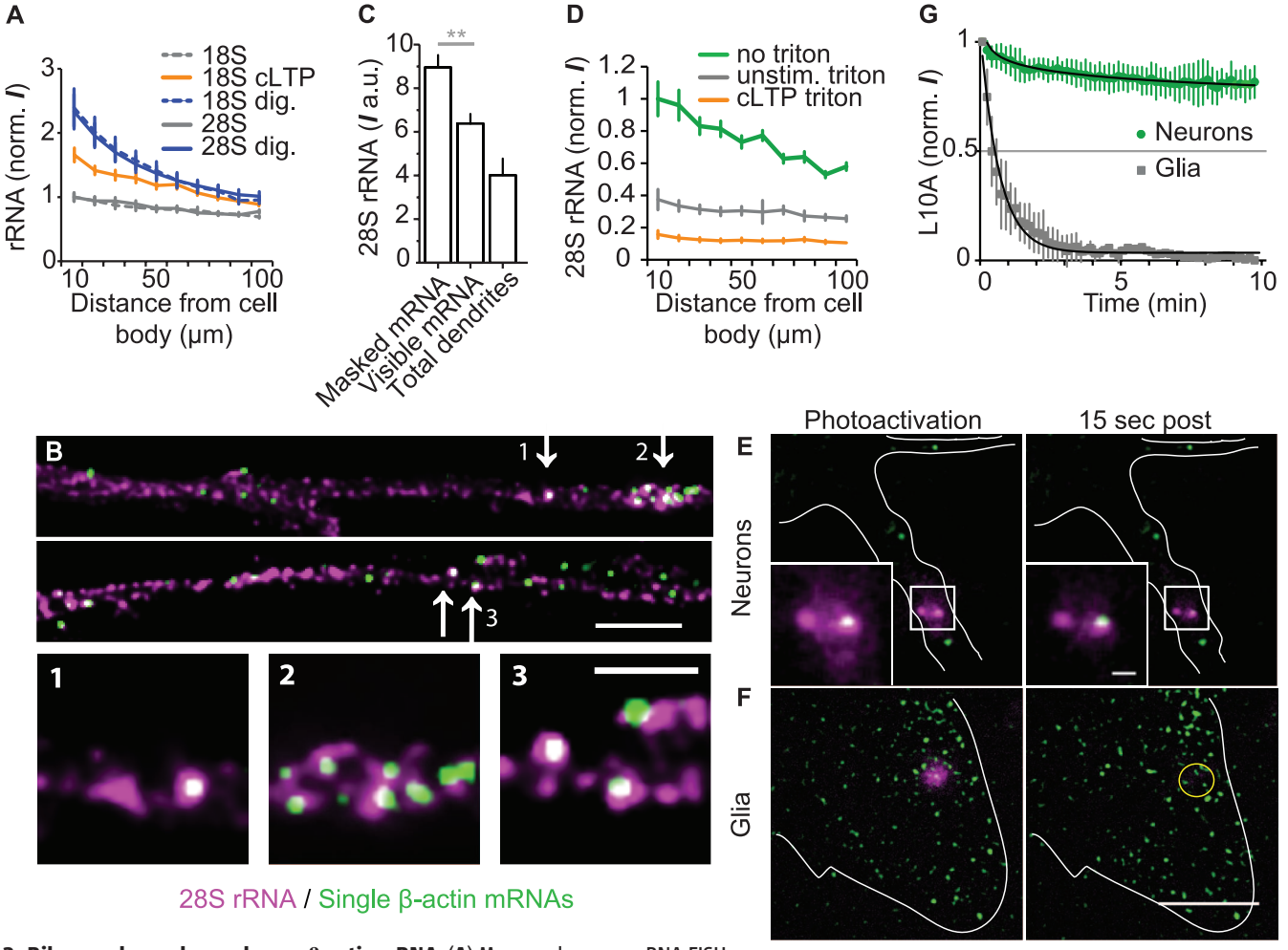

Fig. 2. Ribosomal complexes obscure β-actin mRNA. (**A**) Mean endogenous rRNA FISH fluorescence along dendrites (from top to bottom in key: n = 49, 30, 52, 92, or 97 dendrites). Signal normalized (norm.) to the first point of unstimulated data. Error bars denote SEM. *I*, intensity; dig., digested. (**B**) Single β-actin mRNAs and bright rRNA puncta often coincide (indicated by arrows). Scale bars, 5 μm (upper); 2 μm (lower). Numbers indicate magnified regions in bottom row. Magnified images were resampled with cubic convolution interpolation. (**C**) Mean dendritic ribosome signal surrounding mRNAs and total ribosomal signal (n = 38 dendrites, $^{**}P < 0.01$; Student's t test). a.u., arbitrary units. (**D**) Mean dendritic rRNA FISH fluorescence in prefixative triton digested samples. Error bars indicate SEM. (**E**) Spot photoactivation of L10A-PA-TagRFPt at the site of β-actin mRNA in neurons revealed ribosome structures. Scale bar (inset), 1 μm. (**F**) In glia, L10A diffused away from the activated spot. Scale bar, 10 μm. (**G**) Loss of fluorescent L10A from photoactivated spot (n = 6 glia, 12 neurons). Error bars denote SD.

Three-color imaging differentiated ribosome association with masked and unmasked mRNAs (fig. S5A). β-actin mRNAs hybridized with a second-color probe after protease digestion revealed previously masked mRNAs (about half of the total). Masked mRNAs were associated with brighter ribosomal puncta, supporting the hypothesis that regions rich in ribosomes are part of the same masked complex (Fig. 2C and fig. S5, B to D).

Unbound and unmasked molecules should be washed away during permeablization of live neurons. Puromycin eliminated actively translating polysomes, followed by detergent extraction and fixation (fig. S6A). Large, bright ribosomal puncta were retained in dendrites, some containing single β-actin mRNAs; in contrast, glial cytoplasmic ribosomal signal was extracted (fig. S6, B to D and H). After cLTP in detergent-treated neurons, ribosome and β-actin mRNA FISH signal (Fig. 2D and fig. S6E) and the size of the optically reconstructed ribosomal puncta (fig. S6, F and G) decreased by about half, consistent with increased dispersal of ribosomes and mRNAs as a result of synaptic stimulation.

Increased ribosomal dispersal due to unmasking resulted in increased diffusion of ribosomes and mRNAs. To investigate dendritic rRNA dynamics, we employed spot photoactivation of a ribosomal protein (L10A) fusion. Immobile, bright structures surrounded single mRNAs (Fig. 2E). Photoactivated ribosome fusions exhibited diminished motility in dendrites relative to glial cells (Fig. 2G). After cLTP, quantification of ribosome dispersal from photoactivated sites revealed that the immobile ribosome fraction decreased (fig. S7B). Dendritic β-actin mRNAs were immobile, with a small portion undergoing active transport (*18*). Upon stimulation, immobile mRNAs exhibited corralled diffusion in their local environment (fig. S7, C and D), consistent with degranulation of a complex that prevents mRNA from diffusing until synaptic stimulation.

In addition to increased mRNA and ribosome dynamics, cLTP increased protein synthesis of a reporter for β-actin mRNA, consistent with unmasking that correlates with increased local β-actin translation (fig. S8). The protein FMRP has been shown to be a component of RNA granules and stalls ribosomes on mRNAs (*19*). *Fmr*1 knockout brains exhibit a reduction in the postpolysomal fractions (*20*), suggesting a role for *Fmr*1 in granule integrity. Accordingly, *Fmr*1 knockdown in culture decreased the abundance of masked β-actin mRNAs (fig. S9, A to C). We observed a similar effect in neurons isolated from knockout animals lacking the β-actin mRNA binding protein ZBP1 (fig. S9D).

In the model supported by this work, β-actin mRNA is present all along dendrites and is kept in a dormant state by packaging into inert structures ready to be locally activated. During synaptic stimulation, downstream effectors of signaling pathways locally prompt complex disassembly, putatively allowing active translation of mRNAs at activated synapses. This could be accomplished by regulation of self-aggregating protein motifs through posttranslational modifications (*21*) facilitating cycles of localized RNA granule formation and degranulation, thus making use of the same mRNAs repeatedly over time.

References and Notes

1. S. Ramón y Cajal, *Proc. R. Soc. London* **55**, 444–468 (1894).
2. A. Holtmaat, K. Svoboda, *Nat. Rev. Neurosci.* **10**, 647–658 (2009).
3. M. Matsuzaki, N. Honkura, G. C. Ellis-Davies, H. Kasai, *Nature* **429**, 761–766 (2004).
4. J. Tanaka *et al.*, *Science* **319**, 1683–1687 (2008).
5. B. Ramachandran, J. U. Frey, *J. Neurosci.* **29**, 12167–12173 (2009).
6. M. A. Sutton, E. M. Schuman, *Cell* **127**, 49–58 (2006).
7. T. Eom, L. N. Antar, R. H. Singer, G. J. Bassell, *J. Neurosci.* **23**, 10433–10444 (2003).
8. M. E. Klein, T. J. Younts, P. E. Castillo, B. A. Jordan, *Proc. Natl. Acad. Sci. U.S.A.* **110**, 3125–3130 (2013).
9. I. J. Cajigas *et al.*, *Neuron* **74**, 453–466 (2012).
10. A. M. Krichevsky, K. S. Kosik, *Neuron* **32**, 683–696 (2001).
11. G. Elvira *et al.*, *Mol. Cell. Proteomics* **5**, 635–651 (2006).
12. T. E. Graber *et al.*, *Proc. Natl. Acad. Sci. U.S.A.* **110**, 16205–16210 (2013).
13. Materials and methods are available as supplementary materials on *Science* Online.
14. D. Zenklusen, D. R. Larson, R. H. Singer, *Nat. Struct. Mol. Biol.* **15**, 1263–1271 (2008).
15. W. Lu *et al.*, *Neuron* **29**, 243–254 (2001).
16. Y. Kanai, N. Dohmae, N. Hirokawa, *Neuron* **43**, 513–525 (2004).
17. R. B. Knowles *et al.*, *J. Neurosci.* **16**, 7812–7820 (1996).
18. H. Y. Park *et al.*, *Science* **343**, 422–424 (2014).
19. J. C. Darnell *et al.*, *Cell* **146**, 247–261 (2011).
20. A. Aschrafi, B. A. Cunningham, G. M. Edelman, P. W. Vanderklish, *Proc. Natl. Acad. Sci. U.S.A.* **102**, 2180–2185 (2005).
21. T. W. Han *et al.*, *Cell* **149**, 768–779 (2012).

Acknowledgments: We thank G. J. Bassell for the gift of the Dendra-actin 3′UTR construct, J. Du Hoffmann for invaluable programming help, D. R. Larson for Localize software, and Y. J. Yoon for cloning L10A and helpful discussions. We also thank T. Trćek and other past and present members of the Singer lab for their suggestions and support. This work was supported by NIH grant NS083085-19 (formerly GM84364) and the Weisman Family Foundation. Author notes: A.R.B., B.W., and R.H.S. designed the experiments; A.R.B. performed the experiments; A.R.B. and B.W. performed optical engineering and data analysis; and A.R.B. and R.H.S. wrote the manuscript. Data in this paper are in partial fulfillment of the Ph.D. degree to A.R.B.

Supplementary Materials

www.sciencemag.org/content/343/6169/419/suppl/DC1
Materials and Methods
Figs. S1 to S9
References
FISH Probe Sequences
Movies S1 and S2

9 July 2013; accepted 4 December 2013
10.1126/science.1242939

Visualization of Dynamics of Single Endogenous mRNA Labeled in Live Mouse

Hye Yoon Park,[1,2] Hyungsik Lim,[3] Young J. Yoon,[1] Antonia Follenzi,[4,5] Chiso Nwokafor,[1,3,6] Melissa Lopez-Jones,[1] Xiuhua Meng,[1] Robert H. Singer[1,2,7,8]*

The transcription and transport of messenger RNA (mRNA) are critical steps in regulating the spatial and temporal components of gene expression, but it has not been possible to observe the dynamics of endogenous mRNA in primary mammalian tissues. We have developed a transgenic mouse in which all β-actin mRNA is fluorescently labeled. We found that β-actin mRNA in primary fibroblasts localizes predominantly by diffusion and trapping as single mRNAs. In cultured neurons and acute brain slices, we found that multiple β-actin mRNAs can assemble together, travel by active transport, and disassemble upon depolarization by potassium chloride. Imaging of brain slices revealed immediate early induction of β-actin transcription after depolarization. Studying endogenous mRNA in live mouse tissues provides insight into its dynamic regulation within the context of the cellular and tissue microenvironment.

Recent advances have provided insights into the behavior of RNA in real time (*1*). However, most live-cell imaging techniques require transfection or injection of exogenous reporters that are typically overexpressed or are missing regulatory elements and binding partners present in the endogenous molecules. Moreover, immortalized cells may not accurately exhibit RNA regulation representative of the native tissue environment.

To address these limitations, we generated a transgenic mouse in which all endogenous β-actin mRNA is fluorescently labeled by specific binding between the MS2 bacteriophage capsid protein (MCP) and the MS2 binding site (MBS) RNA stem-loops (*2*). Lentiviral transgenesis (*3*) was used to integrate the MCP-GFP (green fluorescent

[1]Department of Anatomy and Structural Biology, Albert Einstein College of Medicine, Bronx, NY 10461, USA. [2]Gruss-Lipper Biophotonics Center, Albert Einstein College of Medicine, Bronx, NY 10461, USA. [3]Department of Physics and Astronomy, Hunter College and Graduate Center of the City University of New York, New York, NY 10065, USA. [4]Department of Pathology, Albert Einstein College of Medicine, Bronx, NY 10461, USA. [5]Department of Health Sciences, University of Piemonte Orientale "A. Avogadro," Novara, Italy. [6]Department of Biological Sciences, Hunter College and Graduate Center of the City University of New York, New York, NY 10065, USA. [7]Dominick P. Purpura Department of Neuroscience, Albert Einstein College of Medicine, Bronx, NY 10461, USA. [8]Howard Hughes Medical Institute, Janelia Farm Research Campus, Ashburn, VA 20147, USA.

*Corresponding author. E-mail: robert.singer@einstein.yu.edu